Design and Optimization of Dual-Winding Fault-Tolerant Permanent Magnet Motor

Xuefeng Jiang, *Member*, *IEEE*, Shaoshuai Wang, Qiang Li, and Yufei Gao
(Invited)

***Abstract*—To improve the performance of the traditional fault-tolerant permanent magnet (PM) motor, the design and optimal schemes of dual-winding fault-tolerant permanent magnet motor (DWFT-PMM) are proposed and investigated. In order to obtain small cogging torque ripple and inhibiting the short-circuit current, the air gap surface shape of the PM and the anti short-circuits reactance parameters are designed and optimized. According to the actual design requirements of an aircraft electrical actuation system, the parameters, finite element analysis and experimental verification of the DWFT-PMM after optimal design are presented. The research results show that the optimized DWFT-PMM owns the merits of strong magnetic isolation, physics isolation, inhibiting the short circuit current, small cogging torque ripple and high fault tolerance.**

***Index Terms*—Dual-winding motor, design and optimization, fault-tolerance, finite element analysis, short-circuit fault.**

I. Introduction

PERMANENT magnet (PM) motor has been widely used in hybrid electric vehicles, aerospace and other fields because of the merits such as high power density, high torque density, compact structure and high efficiency [1]-[5]. Many scholars have carried out fruitful researches on the working principle of PM motor, electromagnetic performance analysis, mathematical modeling, decoupling control of internal and external motor, driving control technology and so on [6]-[10].

In recent years, the researches on PM fault-tolerant motor have been actualized by scholars. For instance, the three-phase, four-phase, five-phase and six-phase PM fault-tolerant motor have been researched. Meanwhile, the double-channel and three-channel three-phase PM fault-tolerant motor have been carried out. However, each PM fault-tolerant motor and drive system have their own characteristic [11]-[17].

In R. Ma *et al.* [18], the slot and pole combination and winding distribution of six-phase fault-tolerant permanent magnet rim driven motor are theoretically analyzed. The short-circuit current suppression capability and mutual inductance reduction method in different case of slot and pole combination is verified, which provides a valuable for the application of fault-tolerant permanent magnet rim driven motor in ship propulsion field.

J. Zhu et al. [19] describe the novel current vector fault-tolerant control strategy to generate the same output torque and reduce the torque ripples under healthy, winding open-circuit fault and winding short-circuit fault conditions.

H. Bai et al. [20] presents the vector control strategies under healthy and one-phase open-circuit faulty conditions were proposed in which the magnetomotive force was kept constant with the minimum copper loss.

The traditional PM motors always adopt distributed winding. However, this kind of winding type has no the magnetic isolation ability. Once the short-circuit fault occurrence, the winding will be burnt due to short-circuit over-current and the normal phase winding will be influenced by the magnetic field coupling. Moreover, the ripple of electromagnetic torque is increased, and the motor drive system can not work properly. In order to make the motor have magnetic isolation, physical isolation, electrical isolation and thermal isolation, the centralized windings of PM fault-tolerant motor is adopted. However, there are some problems such as high cogging torque ripple, high harmonic content, insufficient sinusoidal of back EMF at present [21]-[25]. Meanwhile, to avoid the amplitude of short-circuit fault over-current, it is necessary that withstand short-circuit current parameters need to be optimized so as to keep current in an appropriate range [26]-[29].

The design and optimization of a dual-winding fault-tolerant permanent magnet motor (DWFT-PMM) is proposed and investigated for improving DWFT-PMM running characteristics in this paper. First, the operation mode and design requirements of DWFT-PMM are introduced. Then, the schemes of design and performance optimization of DWFT-PMM are proposed and investigated. To verify the motor performance, the optimal model is established, and the finite element analysis results are presented in Section IV. In Section V, the DWFT-PMM is manufactured based on the design and optimal results, and the experimental results are rendered. Finally, conclusions are presented.

Manuscript was submitted for review on 31, January, 2019.

This work was supported by the National Natural Science Foundation of China (51807094); the Fundamental Research Funds for the Central Universities (No.30918011327); and the Scientific Research Foundation of Nanjing University of Science and Technology (AE89991/036).

Xuefeng Jiang is with the Nanjing University of Science and Technology.(e–mail: jxf@njust.edu.cn)

Shaoshuai Wang is currently working toward the M.S degree in School of Automation, Nanjing University of Science and Technology(e-mail: 1552008643@qq.com)

Qiang Li is with the Department of Electrical Engineering, School of Automation, Nanjing University of Science and Technology(e-mail: chnliqiang@njust.edu.cn)

Yufei Gao is currently working toward the M.S degree in School of Automation, Nanjing University of Science and Technology

Digital Object Identifier 10.30941/CESTEMS.2019.00007

II. Operation Mode and Design Requirement of DWFT-PMM

A. Operation Mode of DWFT-PMM

According to the requirements of fault-tolerant operation, there are three main operation modes of DWFT-PMM: normal operation mode, open-circuit fault operation mode and short-circuit fault operation mode.

The open-circuit fault operation state and short-circuit fault operation state of DWFT-PMM winding are researched intensively. The fault probability of the aircraft motor drive system per flight hour is illustrated in Table I. The failure rate data of the aircraft motor drive system per flight hour is derived from the Ref. [22]. From the Table I, it can be seen that the high probability of winding open-circuit fault and winding short-circuit fault in flight, so it is the most common fault. Hence, the open-circuit fault and short-circuit fault operation of winding are analyzed mainly in this paper.

TABLE I
PROBABILITY OF MOTOR DRIVE SYSTEM FAULT IN AIRCRAFT FLIGHT

Fault Type	Failure Rate / Per Flight Hour
Motor Winding Open-circuit Fault	1.3×10^{-5}
Connection Point Open-circuit Fault	1×10^{-6}
Other Open-circuit Faults	4×10^{-7}
Motor Winding Short-circuit Fault	6.7×10^{-6}
Connection Point Short-circuit Fault	1×10^{-6}
Other Short-circuit Faults	4×10^{-7}
Total Failure Rate	2.25×10^{-5}

B. Design Requirements of DWFT-PMM

According to the actual requirements of the aircraft electrical actuation system, the design requirements of the DWFT-PMM are shown in Table II.

TABLE II
DESIGN REQUIREMENTS OF DWFT-PMM

Main Design Index	Design Requirement
Rated Power	10 kW
Rated Torque	20 Nm
Rated Speed	5000 rpm
DC Bus Voltage	270V
Rated Point Motor Efficiency	> 80%
No-load Back EMF THD	< 3%
Mutual Inductance/ Self-inductance	< 5%
Cooling Mode	air-cooled
Stable Short-circuit Current/Rated Current	2
Cogging Torque Ripple/Rated torque	< 1%
Stator Rotor Yoke Magnetic Density	< 1.7T
Stator Tooth Density	< 1.8T
Electric Density	< 10A/mm^2
No-load Back EMF Peak	125V
Stator Slot Width	> 0.6 mm
Trough Full Rate	> 0.4

III. Design and Performance Optimizations of DWFT-PMM

According to the design requirements of DWFT-PMM as shown in Table II, the design and performance optimization of DWFT-PMM is carried out. The flow chart of design and performance optimization of DWFT-PMM is shown in Fig 1. The DWFT-PMM has a high per-unit inductance required to limit the short-circuit fault current.

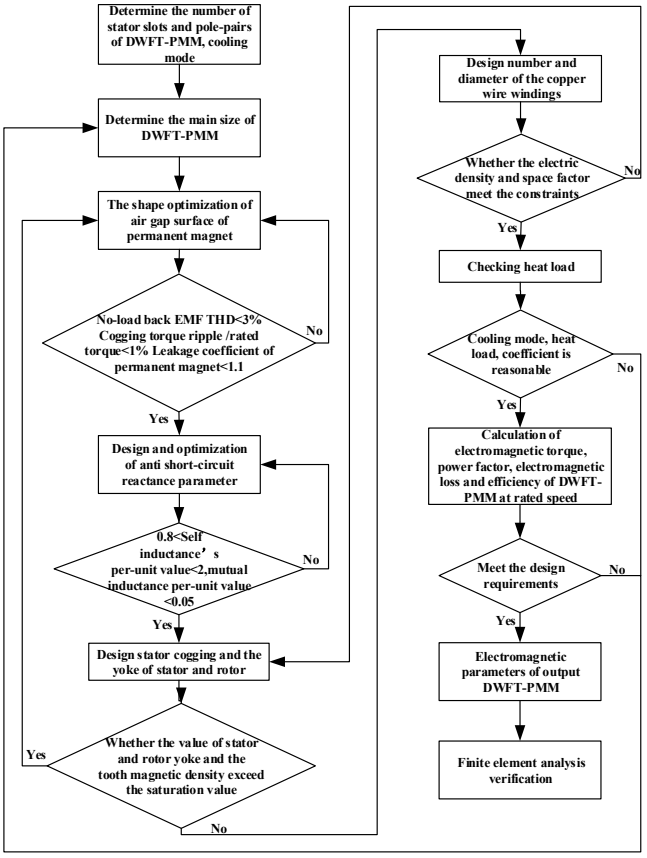

Fig. 1. Flow chart of design and performance optimization of DWFT-PMM

A. PM Air Gap Surface Shape Optimization of DWFT-PMM

In order to solve the problem of the cogging torque ripple, the conventional optimization method is to adopt skewed slots, change slot size or change pole arc coefficient of magnetic steel to improve the sinusoidal degree of no-load back EMF or reduce the cogging torque ripple. However, it is difficult to reduce the cogging torque ripple and increase the sinusoidal degree of no-load back EMF by conventional optimization method at the same time. In this paper, the air gap surface shape of PM is optimized to solve this problem. The PM air gap surface shape optimization of DWFT-PMM is demonstrated in Fig. 2.

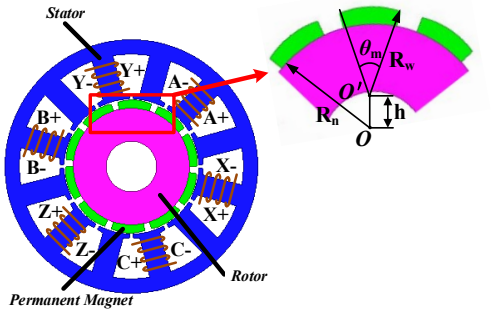

Fig. 2. Optimization of air gap surface shape of PM

It can be seen from Fig. 2 that o, o' are the center of the internal arc and the external arc of rotor magnetic steel respectively. R_n, R_w are the radius of the internal arc and the

external arc of rotor magnetic steel respectively. h is the centrifugal height which is defined as the distance between the center of rotor magnetic steel internal and external arc. Furthermore, θ_m is the rotor magnetic steel external arc radian.

B. Design and Optimization of Anti-short-circuit Reactance Parameters

Due to the magnetic isolation characteristics of DWFT-PMM, the mutual inductance between adjacent phase windings is tiny and the value can be ignored, so the steady-state short-circuit current $\bar{I}_s$ can be expressed as:

$$\bar{I}_s = \frac{\bar{E}_0}{\sqrt{(\omega_e L_s)^2 + R_s^2}} \tag{1}$$

where $\bar{E}_0$ is no-load back EMF, R_s is phase resistance and L_s is phase self-inductance, ω_e is rotor electric angular velocity.

DWFT-PMM phase self-inductance L_s can be expressed as:

$$L_s = L_{sm} + L_{s\sigma} \tag{2}$$

where L_{sm} is phase windings excitation inductance, $L_{s\sigma}$ is phase windings leakage inductance.

Owing to the phase self-inductance L_s of motor is much greater than the phase resistance R_s when the no-load back EMF is fixed. Hence, the resistance can be ignored, and the short-circuit current $\bar{I}_s$ is mainly related to the self-inductive L_s.

In addition, surface structure is applied to the design of PM, thus its phase winding excitation inductance is tiny. The short-circuit current is mainly affected by the leakage inductance of the phase winding in system steady-state. Therefore, the key to optimization of short-circuit current is to design the leakage inductance of phase winding of DWFT-PMM.

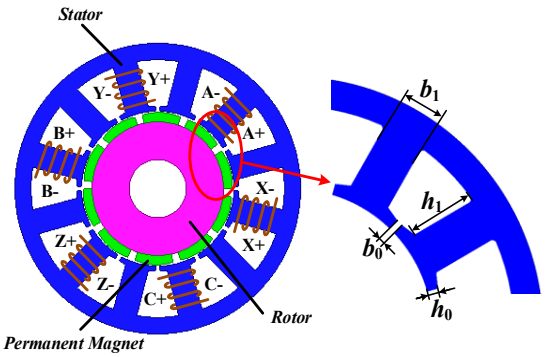

Fig. 3. Optimization of DWFT-PMM stator slot.

The design formula for the leakage inductance of the phase winding can be given as follows:

$$L_{s\sigma} = \frac{\psi_{s\sigma}}{i_{s\sigma}} = \frac{n_0 \phi_{s\sigma}}{i_{s\sigma}} \tag{3}$$

where $i_{s\sigma}$ is winding leakage inductance current, $\psi_{s\sigma}$ is winding leakage inductance flux-linkage, n_0 is winding turns, $\phi_{s\sigma}$ is winding flux.

The leakage inductance flux of the winding can be expressed as:

$$\phi_{s\sigma} = \frac{F_{s\sigma}}{R_0} \tag{4}$$

where $F_{s\sigma}$ is winding leakage inductance magneto motive force, R_0 is reluctance corresponded to $L_{s\sigma}$.

Winding leakage inductance magneto motive force can be expressed as:

$$F_{s\sigma} = n_0 i_{s\sigma} \tag{5}$$

DWFT-PMM phase winding leakage inductance can be simplified as:

$$L_{s\sigma} = \frac{n_0 F_{s\sigma}}{i_{s\sigma} R_0} = \frac{n_0^2}{R_0} \tag{6}$$

The leakage inductance of the winding is concentrated in the leakage inductance of the motor slot, and the slot reluctance can be expressed as:

$$R_{01} = \frac{b_0}{2\mu_0 (b_0 + h_0)(b_0 + l_0)} \tag{7}$$

where R_{01} is slot reluctance, b_0 is the slot width, h_0 is slot thickness, l_0 is effective axial length, μ_0 is air gap permeability.

Combined with (6), the leakage inductance of slot can be expressed as:

$$L_{s\sigma 1} = \frac{2\mu_0 n_0^2 (b_0 + h_0)(b_0 + l_0)}{b_0} \tag{8}$$

where $L_{s\sigma 1}$ is slot leakage inductance.

Obviously, the value of b_0 is far less than the value of l_0, therefore, equation (8) can be simplified as:

$$\begin{aligned} L_{s\sigma 1} &= \frac{2\mu_0 n_0^2 (b_0 + h_0) l_0}{b_0} \\ &= 2\mu_0 n_0^2 l_0 + \frac{2\mu_0 n_0^2 h_0 l_0}{b_0} \end{aligned} \tag{9}$$

According to (9), the slot leakage inductance of the motor phase winding is related to the slot width b_0, the slot thickness h_0 and the effective axial length l_0. The slot leakage inductance of the phase winding increases with the reduction of b_0, the increase of slot thickness of h_0, and the increase of effective axial length of the motor.

To achieve fault-tolerant function of the system and the purpose of reducing the short-circuit current, make the steady-state short-circuit current is twice as the rated current which dual-winding work simultaneously. This means that the steady-state short-circuit current is equivalent to the phase current which outputted 100% power by the single set of winding working, and the motor winding inductance should be designed to 2pu. Hence, it is necessary to increase the leakage inductance of the phase winding. Due to the leakage inductance of the phase winding is mainly concentrated in the leakage inductance of the motor slot, the short-circuit current of the DWFT-PMM can be suppressed by increasing the leakage inductance of the slot.

Hence, as shown in Fig. 3, the deep and narrow slot structure optimization is adopted. The leakage inductance of the slot can be increased effectively, and the DWFT-PMM has a larger stator slot thickness, the magnetic saturation won't occur in the motor under faulty condition, so the possibility of the undesired torque ripples and the decrease of the motor efficiency caused by the magnetic saturation is low. In addition, to make the

effective axial length of the motor as long as possible, the longer core is utilized in structure optimal design.

C. Parameters of DWFT-PMM after Optimal Design

The parameters of DWFT-PMM after optimal design are shown in Table III. Before optimal design, the centrifugal height h of the rotor magnetic steel is 0 mm, the inner arc radius R_n of the rotor magnetic steel is 34.5 mm, and the outer arc radius R_w of the rotor magnetic steel is 39.5 mm. After the air gap surface shape of the permanent magnet is optimized, the centrifugal height h is designed to 10 mm, the inner arc radius R_n of the DWFT-PMM motor rotor magnetic steel is 34.5 mm, the outer circular arc radius of the rotor magnetic steel is 29.5mm, and the arc radian θ_m of the rotor magnetic steel is π/6 rad.

TABLE III
MOTOR PARAMETERS AFTER OPTIMIZATION

Main Design Index	Design Parameters
Stator External Diameter	150mm
Stator Internal Diameter	81mm
Rotor Core External Diameter	69mm
Rotor Core Internal Diameter	50mm
Motor Effective Axial Length	150mm
Air Gap Length	1mm
Rated Torque	20Nm
Stator teeth	12
Magnet poles	10
Phase Winding Turns	24
PM Material	Sm_2Co_{17}
Magnetic Steel Inner Arc Radius *Rn*	34.5mm
Magnetic Steel Outer Arc Radius *Rw*	29.5mm
Magnetic Steel Centrifugal Height *h*	10mm
External Arc Radians *θm*	π/6 rad
Stator Slot Width b_0	2.4mm
Stator Slot Thickness h_0	3.75mm
Stator Tooth Height h_1	22.3mm
Stator Tooth Width b_1	12.5mm
Phase Resistor	0.01Ω
Self-induction	0.42mH
Main Magnetic Flux	0.05Wb

Fig. 4(a) and Fig. 4(b) show the contrast waveforms of cogging torque and air gap radial magnetic density between traditional PM fault-tolerant motor and the optimized DWFT-PMM respectively.

It can be seen that the cogging torque ripple can be decreased effectively due to the optimal design of DWFT-PMM and the sinusoidal degree of air gap radial magnetic density is improved effectively, so that the no-load back EMF sinusoidal degree can be optimized evidently.

IV. FINITE ELEMENT ANALYSIS VERIFICATION

The main parameters of the DWFT-PMM after the performance optimization design are shown in Table III. The finite element model and the finite element grid subdivision diagram of the DWFT-PMM are modeled and verified based on the finite element simulation software ANSOFT MAXWELL, which is shown in Fig. 5. Fig. 5(a) is the finite element model of DWFT-PMM, and Fig. 5(b) is the finite element grid subdivision diagram of DWFT-PMM.

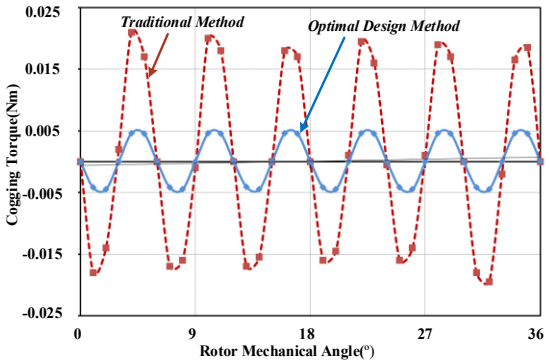

(a) The waveforms of cogging torque,

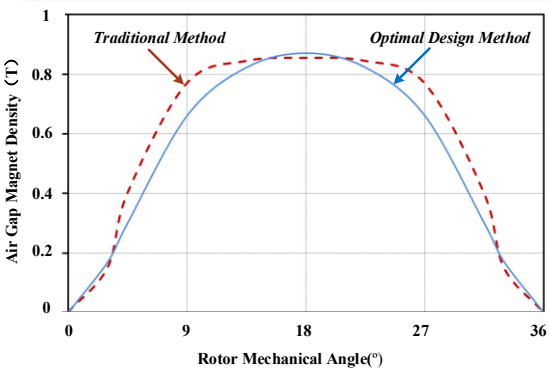

(b) The waveforms of air gap magnetic density.

Fig. 4 Contrast waveforms between traditional PM fault-tolerant motor and the DFPM after optimal design, (a) The waveforms of cogging torque, (b) The waveforms of air gap magnetic density.

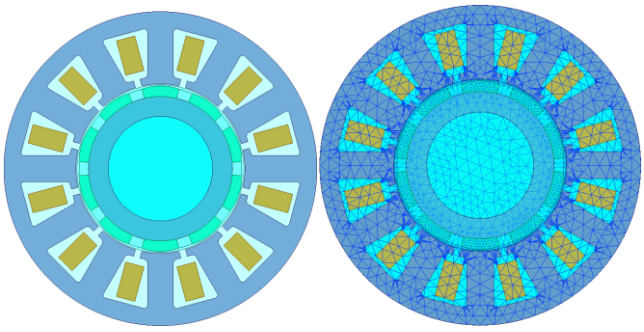

(a) (b)

Fig. 5. Finite element model and finite element grid subdivision of DWFT-PMM, (a) Finite element model, (b) Finite element grid subdivision.

A. Inductance Characteristic

The self-inductance and mutual inductance curves of DWFT-PMM windings are shown in Fig. 6, in which L [A, A] is the self-inductance of phase-A winding and L [A, B] is the mutual inductance between phase-A and phase-B. It can be seen from the diagram that the mutual inductance between windings is less than 5% of winding self-inductance. Hence, the influence of the windings mutual-inductance can be ignored and the motor has the ability of magnetic isolation.

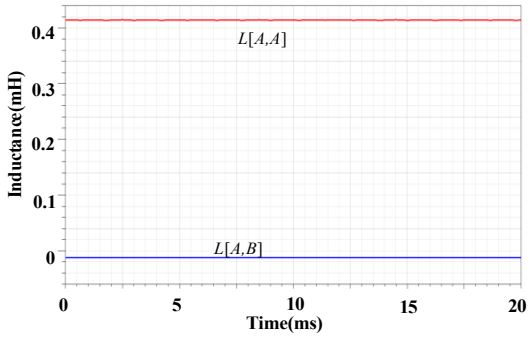

Fig. 6. Self-inductance and mutual inductance curves of DWFT-PMM winding.

B. Cogging Torque Ripple

The waveform of cogging torque ripple of DWFT-PMM after optimal design is shown in Fig. 7. The cogging torque ripple of DWFT-PMM is ±0.01 Nm, its peak value is less than 1% of the motor rated torque, which meets the design requirements. Therefore, the cogging torque ripple is decreased evidently, and the output performance of the motor is good.

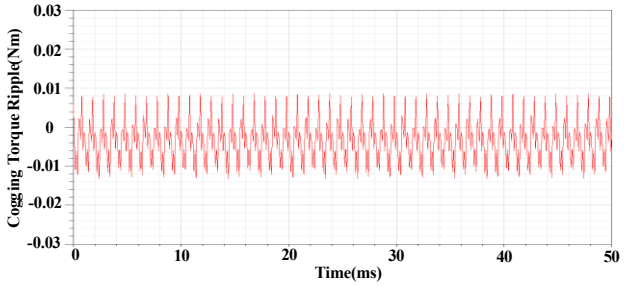

Fig. 7. The waveform of DWFT-PMM cogging torque ripple.

C. No-load Back EMF

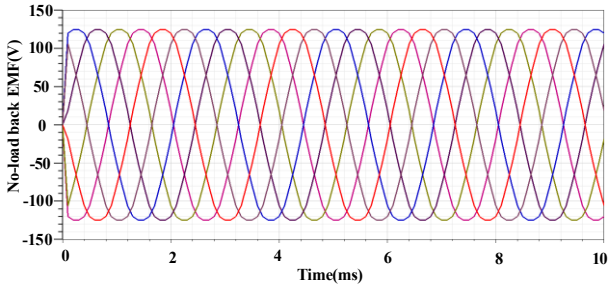

(a) No-load back EMF

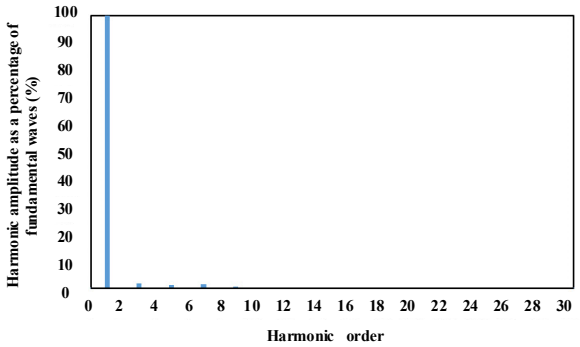

(b) FFT analysis.

Fig. 8. The waveform of no-load back EMF and FFT analysis, (a) No-load back EMF, (b) FFT analysis.

The back EMF waveform of DWFT-PMM and its fast Fourier transform (FFT) analysis are shown in Fig. 8. The figure shows that the back EMF has a good sinusoidal degree, and the peak value of back EMF is 125V. The total harmonic distortion coefficient (THD) is 2.55%, which meets the design requirements of DWFT-PMM.

D. Short-circuit Current

The current waveform of short-circuit fault in DWFT-PMM phase-A winding is shown in Fig. 9. At this time, the short-circuit current of the winding will be attenuated in the form of exponential function. Finally, the peak value stabilized around 53A. It is equivalent to the current value of 100% power output for single set of winding, which meets the requirements of fault-tolerant design and makes the DWFT-PMM have the strong ability to suppress the short-circuit current.

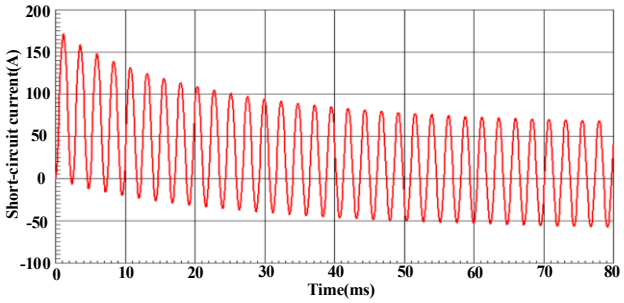

Fig. 9. The waveform of short-circuit current.

E. Electromagnetic Torque

The electromagnetic torque waveform of DWFT-PMM is shown in Fig. 10. Because the design rated torque of the DWFT-PMM is 20Nm, each sets of windings only needs to provide 50% power in dual-winding running mode. After fault occurs in winding, in order to keep the system output 100% power, the motor operates in single winding running mode by removing the fault-winding, and the current value of the remaining normal single-winding needs to be increased by twice as the original current. As a result, the output torque of system is consistent.

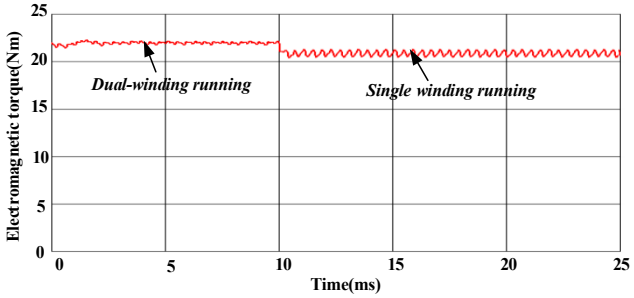

Fig. 10. The waveform of electromagnetic torque

It can be seen from Fig. 10 that the maximum output electromagnetic torque of 21.5Nm can be obtained when the motor operates in dual-winding running mode. When the motor operates in single winding running mode, the maximum output electromagnetic torque is 20.5Nm. Hence, it can meet the design requirements of rated torque 20Nm. Moreover, the electromagnetic torque ripple of motor is ±0.5 Nm and the peak value of torque ripple is less than 5% of the rated torque. At the same time, the output torque of the DWFT-PMM is basically

unchanged when the operation mode switching from the state of dual-winding running simultaneously to the single set of winding running, which has the capability of realizing the fault-tolerant control for the system.

F. Loss Analysis

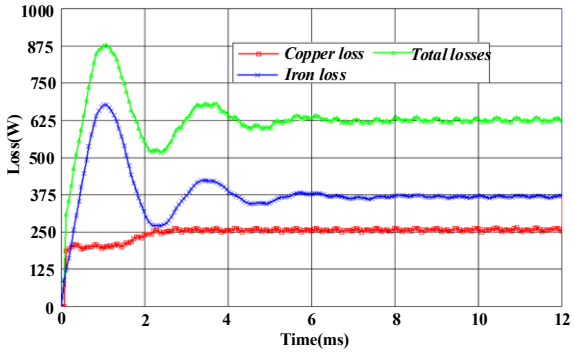

Fig. 11. The waveform of loss analysis

The copper and iron losses of DWFT-PMM are shown in Fig. 11 when the motor running under rated operation conditions. With the addition loss of motor, the copper loss of DWFT-PMM is about 255 W, the iron loss is about 370 W, and the total loss is about 625W. Compared with the rated power 10kW, the total efficiency of DWFT-PMM is about 93.75%, which meets the design requirements of DWFT-PMM.

G. Analysis of Open-circuit Fault in Phase-A

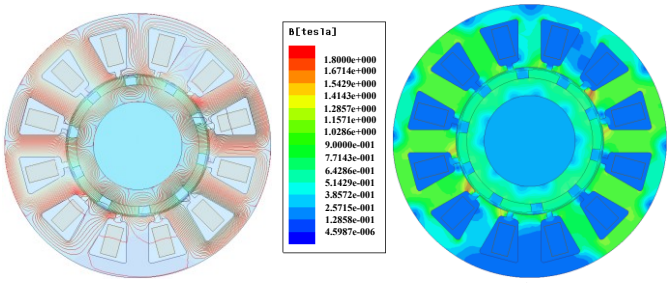

(a) (b)

Fig. 12. Magnetic field line and magnetic density distribution when open-circuit faults in phase-A winding. (a) Magnetic field line distribution. (b) Magnetic density distribution.

It can be seen from Fig. 12(a) that almost no coupling of magnetic field lines among the phase windings, and open-circuit fault have little effect on other phases. It can be explained that the optimal DWFT-PMM possesses strong magnetic isolation ability under the state of open-circuit fault. Moreover, as shown in Fig. 12(b), the magnetic density of yoke is not greater than 1.3 T and the stator teeth magnetic density is less than 1.7 T. Hence, even in the condition of open-circuit fault, it still meets the design requirements of material magnetic density saturation.

H. Analysis of Short-circuit Fault in Phase-A

Due to the type of DWFT-PMM winding is single-layer centralized armature winding, the short-circuit fault at the end of the armature winding is the most common fault.

Taking the phase-A winding as an example, when short-circuit fault occurs at the end of phase-A armature winding, the magnetic field line and magnetic density distribution are shown in Fig. 13. Fig. 13(a) is magnetic field line distribution and Fig. 13(b) is magnetic density distribution.

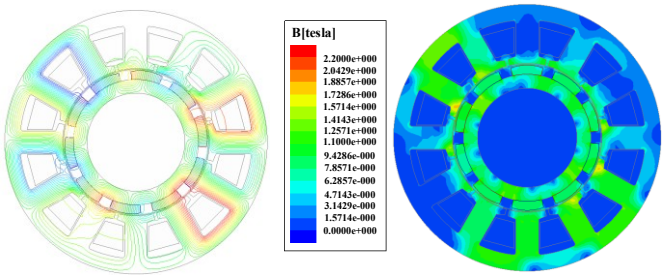

(a) (b)

Fig. 13. Magnetic field line and magnetic density distribution of short-circuit faults in phase-A winding, (a) Magnetic field line distribution. (b) Magnetic density distribution.

It can be seen from Fig. 13(a) that almost no coupling of magnetic field lines among the phase windings, and there is almost no magnetic field line in phase-A short-circuit fault winding. It can be explained that the optimal DWFT-PMM has good magnetic isolation ability under the state of short-circuit fault. As shown in Fig. 13(b), the magnetic density of yoke is not greater than 1.6 T and the stator teeth magnetic density is less than 1.8 T. In the condition of short-circuit fault, it still meets the design requirements of material magnetic density saturation.

V. Experimental Verification

The 10 kw DWFT-PMM prototype is shown in Fig. 14. And Fig. 14 (a) is internal stator structure of the DWFT-PMM. Fig. 14 (b) is prototype appearance design of DWFT-PMM.

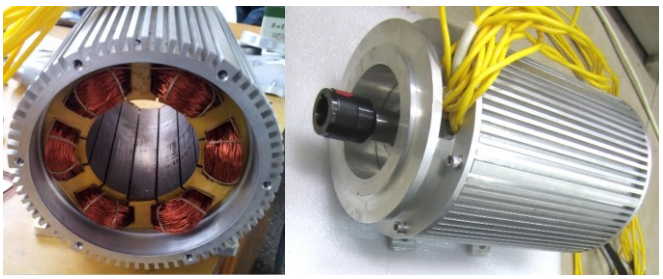

(a) (b)

Fig. 14. DWFT-PMM prototype. (a) Internal stator structure, (b) Prototype appearance design.

A. Experimental Measurement of No-Load Back EMF and Back EMF Harmonic

In order to verify the theoretical analysis of the design and performance optimization of DWFT-PMM, the no-load back EMF of DWFT-PMM is investigated. The DWFT-PMM is driven by the prime mover and the winding of each phase is open-circuit state, the terminal voltage of the phase-*A* winding is measured, it is equal to the no-load back EMF of the motor.

The no-load back EMF waveform of phase-*A* winding experimental value and finite element analysis when the optimized DWFT-PMM is running at the 2000r/min are shown in Fig. 15. The experimental THD is 2.24%, which meets the design requirements of DWFT-PMM. It can be seen that the no-load back EMF possess good sinusoidal degree and the experimental results agree well with the finite element analysis

results, therefore the correctness of the finite element analysis is verified.

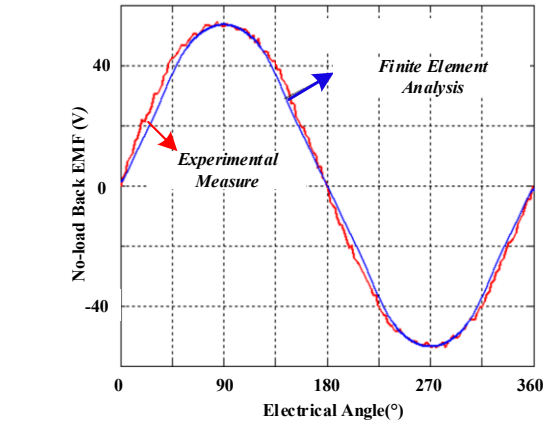

(a)

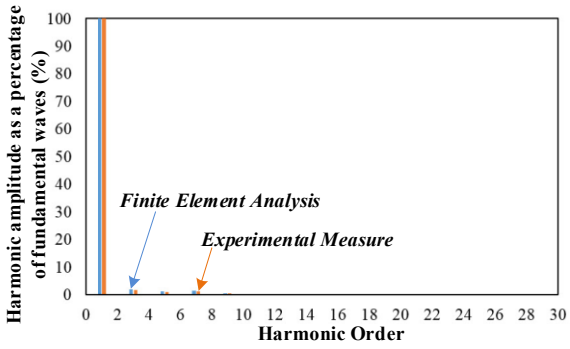

(b)

Fig. 15. Experimental results of No-Load Back EMF and Back EMF Harmonic, (a) The waveforms of no-load back EMF, (b) Back-EMF harmonics analyzed by experiment and finite element analysis.

B. Experimental Measurement of Inductance and Resistance

The inductance and resistance of motor are tested by HP4284A precision LCR tester. The results of finite element simulation and experiments about inductance are shown in Table IV. Due to the symmetry of DWFT-PMM, the self-inductance of phase-A winding, the self-inductance of phase-X winding and the mutual inductance between phase-A and phase-B windings are measured.

TABLE IV
THE RESULTS OF MOTOR WINDING INDUCTANCE TESTED BY FINITE ELEMENT SIMULATION AND EXPERIMENTAL

	L_{AA}	L_{AB}	L_{XX}
Finite element simulation (mH)	0.418	-0.017	0.418
Experimental test (mH)	0.426	0.01	0.423

Due to the direction of induction is opposite to the prescribed positive direction, the finite element simulation value of mutual inductance between A-B phase windings is negative. It can be seen from the Table IV that the finite element simulation results of winding inductance are similar to the experimental results, the correctness of the finite element analysis can be verified. The motor resistance can be read directly, the test value is 0.012Ω, which is consistent with the theoretical value of the design basically.

C. Experimental Measurement of Short-Circuit Current

After the optimal design of the stator slot, the leakage inductance of the slot is increased effectively, thus the short-circuit current is restrained, the purpose of reducing the short-circuit current is realized, and the short-circuit current is kept in the range of actual operation need.

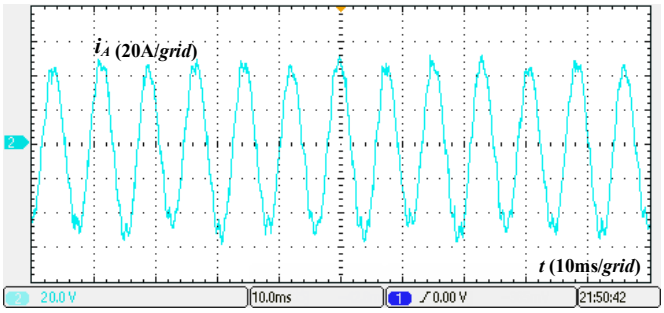

Fig. 16. Experimental waveform of phase-*A* short-circuit current.

Phase-*A* winding short-circuit current of optimized DWFT-PMM is shown in Fig. 16. It can be seen that the measured peak value of the winding short-circuit current is stable at about 45A, which is almost equal to the current when the single set of winding running under the 100% out-put power condition.

It is in the range of the motor bearing ability; the motor will not be damaged and the fault-tolerant design requirements will be satisfied. Therefore, the DWFT-PMM has the ability to restrain short-circuit current.

D. Experimental Measurement of Electromagnetic Torque

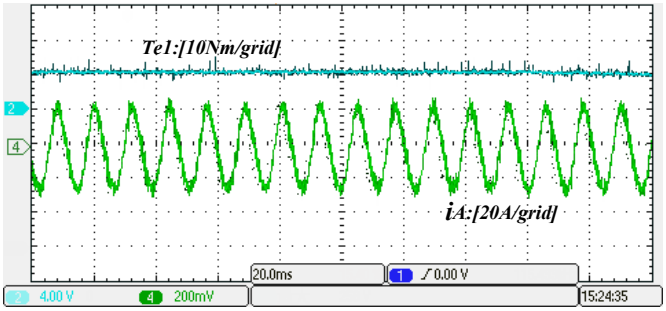

Fig.17. Experimental results of electromagnetic torque and phase-A current.

The experimental results of electromagnetic torque and phase-A current are shown in Fig. 17. The torque value of *ABC* windings is stabilized at 10Nm under the rated load condition. The current peak value of phase-A winding is about 26A. It can be seen from the Fig. 17 that the output torque after the optimized design of the DWFT-PMM has a small torque ripple. Hence, it can be concluded that the DWFT-PMM has a good torque performance and it can meet the design requirements of rated torque.

VI. CONCLUSION

In this paper, the schemes of design and performance optimization of DWFT-PMM are proposed and investigated. In terms of the actual requirements of the aircraft electrical actuation system, the flow chart of design and performance optimization of DWFT-PMM is established. Then, the air gap surface shape of the PM and the anti short-circuits reactance

parameters are designed and optimized. The parameters of DWFT-PMM after optimal design are obtained. Moreover, the performance of optimal DWFT-PMM is verified by finite element analysis from the aspects of inductance characteristic, cogging torque ripple, no-load back EMF, short-circuit current, electromagnetic torque and loss analysis. Finally, the experimental verification of DWFT-PMM prototype is presented. The results show that the optimized DWFT-PMM owns the merits of strong magnetic isolation, physics isolation, inhibiting the short circuit current, small cogging torque ripple and high fault tolerance. The DWFT-PMM will have wide application prospect in aerospace.

REFERENCES

[1] W. Zhao, B. Wu, Q. Chen, et al. "Fault-tolerant direct thrust force control for a dual inverter fed open-end winding linear vernier permanent-magnet motor using improved SVPWM," *IEEE Transactions on Industrial Electronics*, 2018, 65(9): 7458-7467.

[2] M. Cheng, P. Han, G. Buja, et al. "Emerging multi-port electrical machines and systems: past developments, current challenges and future prospects," *IEEE Transactions on Industrial Electronics*, 2018, 65(7): 5422-5435.

[3] W. Zhao, L.Xu, G. Liu. "Overview of permanent-magnet fault-tolerant machines: Topology and design," *IEE CES Transactions on Electrical Machines and Systems*, 2018,2(1):51-64.

[4] H. Guo, J. Xu, and Y. Chen, "Robust control of fault-tolerant permanent-magnet synchronous motor for aerospace application with guaranteed fault switch process," *IEEE Transactions on Industrial Electronics*, 2015, 62(12), 7309–7321.

[5] D. Wu and Z. Q. Zhu, "Design tradeoff between cogging torque and torque ripple in fractional slot surface-mounted permanent magnet machines," *IEEE Transactions on Magnetics*, vol. 51, no. 11, pp. 1-4, Nov. 2015.

[6] W. Zhao, M. Cheng, K. T. Chau, R. Cao, and J. Ji, "Remedial injected-harmonic-current operation of redundant flux-switching permanent-magnet motor drives," *IEEE Transactions on Industrial Electronics*, vol. 60, no. 1, pp. 151–159, Jan.2013.

[7] Y. Zhou, X. Lin, and M. Chen, "A fault-tolerant direct torque control for six-phase permanent magnet synchronous motor with arbitrary two opened phases based on modified variables," *IEEE Transactions on Energy Conversion*, vol. 31, no. 2, pp. 549–556, Jun. 2016.

[8] A. Kalimov and S. Shimansky, "Optimal design of the synchronous motor with the permanent magnets on the rotor surface," *IEEE Transactions on Magnetics,* vol. 51, no. 3, pp. 1-4, March 2015.

[9] S. Saha, G. Choi and Y. Cho, "Optimal rotor shape design of LSPM with efficiency and power factor improvement using response surface methodology," *IEEE Transactions on Magnetics*, vol. 51, no. 11, pp. 1-4, Nov. 2015.

[10] Z. Xue, H. Li, Y. Zhou, N. Ren and W. Wen, "Analytical prediction and optimization of cogging torque in surface-mounted permanent magnet machines with modified particle swarm optimization," *IEEE Transactions on Industrial Electronics*, vol. 64, no. 12, pp. 9795-9805, Dec. 2017.

[11] F. Parasiliti, M. Villani, S. Lucidi, and F. Rinaldi, "Finite-element-based multi-objective design optimization procedure of interior permanent magnet synchronous motors for wide constant-power region operation," *IEEE Transactions on Industrial Electronics*, vol. 59, no. 6, pp. 2503–2514, Jun. 2012.

[12] S. G. Min and B. Sarlioglu, "Design optimization of surface permanent magnet machines with fractional slot concentrated windings," 2015 9th International Conference on Power Electronics and ECCE Asia (ICPE-ECCE Asia), Seoul, 2015, pp. 707-713.

[13] P. Alotto, M. Barcaro, N. Bianchi, and M. Guarnieri, "Optimization of interior PM motors with Machaon rotor flux barriers," *IEEE Transactions on Magnetics*, vol. 47, no. 5, pp. 958–961, May 2011.

[14] X. Jiang, W. Huang, R. Cao, Z. Hao, J. Li, and W. Jiang, "Analysis of a dual-winding fault-tolerant permanent magnet machine drive for aerospace applications," *IEEE Transactions on Magnetics*, vol.51, no.11, pp.1- 4, Nov. 2015..

[15] X. Jiang, W. Huang, R. Cao, Z. Hao, and W. Jiang, "Electric drive system of dual-winding fault-tolerant permanent magnet motor for aerospace applications," *IEEE Transactions on Industrial Electronics*, vol. 62, no.12, pp. 7322–7330, Dec.2015.

[16] J. H. Lee, J. Kim, J. Song, D. Kim, Y. Kim and S. Jung, "Distance-based intelligent particle swarm optimization for optimal design of permanent magnet synchronous machine," *IEEE Transactions on Magnetics*, vol. 53, no. 6, pp. 1-4, June 2017.

[17] W. Zhao, J. Kwon, X. Wang, T. A. Lipo and B. Kwon, "Optimal Design of a Spoke-type Permanent Magnet Motor with Phase-group Concentrated-coil Windings to Minimize Torque Pulsations," *IEEE Transactions on Magnetics*, vol. 53, no. 6, pp. 1-4, June 2017.

[18] R. Ma, J. Zhu, Q. Lin and X. Xu, "Investigation on Slot and Pole Combination Schemes for Six-phase Fault-Tolerant Permanent Magnet Rim Driven Motor," *2018 IEEE Student Conference on Electric Machines and Systems*, Hu Zhou, China, 2018, pp. 1-5.

[19] J. Zhu, H. Bai, X. Wang and X. Li, "Current Vector Control Strategy in a Dual-Winding Fault-Tolerant Permanent Magnet Motor Drive," in *IEEE Transactions on Energy Conversion*, vol. 33, no. 4, pp. 2191-2199, Dec. 2018.

[20] H. Bai, J. Zhu, J. Qin and J. Sun, "Fault-tolerant control for a dual-winding fault-tolerant permanent magnet motor drive based on SVPWM," in *IET Power Electronics*, vol. 10, no. 5, pp. 509-516, 21 4 2017.

[21] Z. Haifeng, D. Zhi and Z. Jinghua, "Optimization design and analysis of permanent magnet synchronous motor based on VC," 2017 20th International Conference on Electrical Machines and Systems (ICEMS), Sydney, NSW, 2017, pp. 1-4.

[22] W. Cao, B. C. Mecrow, G. J. Atkinson, J. W. Bennett, and D. J. Atkinson, "Overview of electric motor technologies used for more electric aircraft," *IEEE Transactions on Industrial Electronics*, vol. 59, no. 9, pp. 3523-3531, Sep.2012.

[23] J. J. H. Paulides, B. L. J. Gysen, K. J. Meessen, Y. Tang, and E. A. Lomonova, "Influence of multiple air gaps on the performance of electrical machines with (semi) Halbach magnetization," *IEEE Transaction on Magnetics*, vol. 47, no. 10, pp. 2664–2667, Oct. 2011.

[24] W. Zhao, M.Cheng, K.T.Chau, W.Hua, H. Jia, J. Ji, and W. Li, "Stator-flux-oriented fault-tolerant control of flux-switching permanent-magnet motors," *IEEE Transactions on Magnetics*, vol. 47, no. 10, pp. 4191–4194, Oct. 2011.

[25] X. Liu and W. Fu, "Optimal structure design of permanent magnet motors based on a general pattern of rotor topologies," 2017 IEEE International Magnetics Conference (INTERMAG), Dublin, 2017, pp. 1-1.

[26] S. A. S. Seadati and A. H. Niasar, "Optimal design and finite element analysis of a high speed, axial-flux permanent magnet synchronous motor," 2018 9th Annual Power Electronics, Drives Systems and Technologies Conference (PEDSTC), Tehran, 2018, pp. 133-138.

[27] Y. Shen and Q. Lu, "Design and analysis of linear hybrid-excited slot permanent magnet machines," *IEEE Transactions on Magnetics*, vol. 54, no. 11, pp. 1-6, Nov. 2018.

[28] Y. Kong, M. Lin, R. Guo, N. Li and D. Xu, "Design and optimization of an outer-rotor permanent magnet synchronous machine with an amorphous stator core," *IEEE Transactions on Applied Superconductivity*, vol. 28, no. 3, pp. 1-5, April 2018.

[29] X. Jiang, Q. Li, W. Huang, and R. Cao. "A dual-winding fault-tolerant motor drive system based on the redundancy bridge arm," *IEEE Transactions on Industrial Electronics*, vol. 66, no. 1, pp. 654-662, 2019.

Xuefeng Jiang (S'15-M'17) received the B.S. degree in electrical engineering from Southwest Jiaotong University, Chengdu, China, in 2011, and the Ph.D. degrees in electrical engineering from Nanjing University of Aeronautics and Astronautics, Nanjing, China, in 2017.

Since 2017, he has been with the

Nanjing University of Science and Technology, where he is currently a lecturer with the Department of Electrical Engineering, School of Automation. He has authored or coauthored more than 20 technical papers. He is the holder of more than 20 issued patents. His teaching and research interest include design and control for electric machines, fault diagnosis, and fault-tolerant control for electric drive systems.

Shaoshuai Wang was born in Zaozhuang, Shandong Province, China, in 1995. He received B.S degree in electrical engineering and automation from Qingdao University of Science and Technology, Qingdao, China, in 2017 and he is currently working toward the M.S degree in School of Automation, Nanjing University of Science and Technology, China. His research interests include drive of fault-tolerant permanent-magnet motor and their fault analysis.

Qiang Li was born in Jiangsu Province, China, in1969. He received the B.S. degree in automatic control from Harbin Institute of Technology, Harbin, China, in 1992, and the Ph.D. degree in electrical engineering from Southeast University, Nanjing, China, in 2005.

In 2005, he joined the Department of Electrical Engineering, School of Automation, Nanjing University of Science and Technology, where he has been engaged in teaching and research in the field of electrical engineering. His main research interests include control and drive for electrical machine, switching mode power supply, and embedded systems.

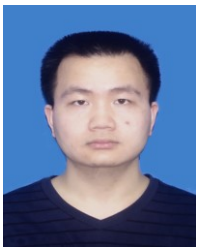

Yufei Gao was born in Zhenjiang, Jiangsu Province, China, in 1995. He received B.S degree in electrical engineering and automation from South-east University, Nanjing, China, in 2017 and he is currently working toward the M.S degree in School of Automation, Nanjing University of Science and Technology, China. His research interests include drive of fault-tolerant permanent magnet motor and their fault analysis.